



# The AC conductivity and dielectric permittivity for PVA-treated MWCNT electrolyte composite

Huda AlFannakh<sup>1,\*</sup>  and S. S. Ibrahim<sup>2</sup>

<sup>1</sup> Physics Department, College of Science, King Faisal University, P.O. Box 400, Al-Ahsa, Saudi Arabia

<sup>2</sup> Physics Department, Faculty of Science, Cairo University, Giza, Egypt

Received: 20 May 2022

Accepted: 4 September 2022

Published online:

17 October 2022

© The Author(s) 2022

## ABSTRACT

Three-phase polymer electrolyte nanocomposite composed of polyvinyl-alcohol (PVA), manganese(II) chloride (MnCl<sub>2</sub>), and multiwall carbon nanotubes (MWCNTs) were prepared using the cast techniques. Impedance spectroscopy was used to investigate the AC electrical conductivity ( $\sigma_{ac}$ ) of two- and three-phase samples with different weight ratios of multiwall carbon nanotubes (MWCNTs) over a wide frequency range and at various fixed temperatures (30 °C to 120 °C). The frequency-dependent nature of  $\sigma_{ac}$  was seen to follow Jonscher's power law. The redistribution of accumulated charges was used to explain the change in the pre-exponent ( $n$ ) and the constant ( $A$ ) after the percolation threshold. As the temperature approached the glass transition temperature, the mobility of ions and polymeric chains also played an important role in this change. The Correlated Barrier Hopping (CBH) model was considered as the most predicted model for the samples at temperatures below 100 °C. However, the Quantum Mechanical Tunneling (QMT) model was predicted to be the most prevalent conduction model for temperatures greater than 100 °C. The values of the activation energy calculated from both  $Z''$  and  $M''$  are mostly close. Equivalent circuits were used to analyze the impedance spectra of the two- and three-phase samples. An attempt was made to explain the impedance behavior of the samples through the elements participating in the equivalent circuits.

## 1 Introduction

Electrolytic polymers represent one of the materials which attract the interest of many researchers because of their potential applications in solid-state batteries, chemical sensors, solar cells, and electrolyte gate transistors [1–16]. The electrolytic polymers are

characterized by their high ionic properties, good mechanical properties, low electrochemical stability, low cost, ease of handling, easy manufacturing as thin films, and it is environmentally friendly. The development of polymers is not only by the addition of some kind of salts for polymers to form polymer electrolyte, but also the researchers have observed

Address correspondence to E-mail: halfannakh@kfu.edu.sa

that the addition of nanomaterials (metals, semiconductors, organic and inorganic, fibers, and oxides, as well as carbon nanotubes) can contribute to improving some physical and/or chemical properties of the polymer electrolyte. This three-phase electrolytic nanocomposite may have specific properties which will be useful in technological applications such as supercapacitors sensors and actuators [17–21].

The improvement of the physical properties of the polymer electrolyte can be through adding carbon nanomaterials (Carbon nanoparticles [22, 23], Carbon nanofibers [24–26], multiwall carbon nanotubes MWCNTs [27–30], etc.[31, 32]), or by addition of ceramic nanomaterials (ZnO [33, 34], TiO<sub>2</sub> [35, 36], BaTiO<sub>3</sub> [37, 38], MnO<sub>2</sub> [39, 40], etc.) or using a conductive polymer as third phase (PANi [41], P3OT [42], etc.).

Polyvinyl alcohol (PVA) electrolyte has been used as basic material for the preparation of three-phase nanocomposite. In the field of energy-storage devices, polyaniline-based electrodes are solidified in the H<sub>2</sub>SO<sub>4</sub>-polyvinyl alcohol gel electrolyte. This two-phase electrolyte was used to construct paper-like polymer supercapacitors using MWCNTs (as the third phase) [43]. Pan et al. [44] investigate the effect of CNTs on the ionic conductivity of the potassium hydroxide (KOH)-doped PVA/CNT membrane. The ionic conductivity increased by adding the functionalized CNT. They found that the methanol permeability was suppressed in the three-phase samples (PVA/KOH/CNTs) compared with the polymer electrolyte two-phase samples (PVA/KOH). Tu et al. [45] used PVA/Li<sub>2</sub>SO<sub>4</sub>/BMIMI gel polymer electrolyte to construct activated carbon-based supercapacitors. They investigate the prepared supercapacitors using cyclic voltammetry, galvanostatic charge–discharge, impedance spectroscopy techniques, and mechanical performance. Such flexible supercapacitors show better cyclic durability and excellent mechanical implementation. A wearable electronic textile three-phase nanocomposite based on PVA/SWCNTs humidity sensor was investigated by Zhou et al. [46]. For the application of Lithium-ion capacitors (LICs), poly(vinylidene fluoride-hexafluoropropylene) (PVDF-HFP) co-doped with multi-walled carbon nanotubes (MWCNT) via weak bond interactions of gel polymer electrolytes (GPEs) was investigated by Shengrui Yu et al. [47]. MWCNTs/PANI electrolyte composites were synthesized by the in situ polymerization technique. Under optimal

conditions, the electrolyte with 4% MWCNTs/PANI and a salt concentration of 0.5 g showed a higher ionic conductivity of 197.4 μS/cm. The ionic conductivity of electrolytes affects the photovoltaic performance of fabricated dye-sensitized solar cells [48]. The dynamics of ionic transport and thermoelectric properties of a methacrylate-based polymer blend in combination with a lithium salt and MWCNTs was investigated by Maximilian Frank et al. [49]. The addition of MWCNTs to the polymer electrolyte allows for variation of the Seebeck coefficient as well as the ionic and electronic conductivities.

A remarkable increase in the electrical resistance of a fiber sensor increases significantly after spraying water. Samples prepared using 1:5 weight ratios of SWCNTs/PVA showed high sensitivity in high relative humidity. Three-phase system composed of MnCl<sub>2</sub>, PVA and PEG with different weight percentages of MnCl<sub>2</sub> was prepared and investigated using Hall measurements [50]. Electrical conductivity of the composite increases with increasing the salt wt.%. The calculated activation energies were decreased with increasing salt wt.%. Dielectric measurement was also investigated for PVA: PEG/MnCl<sub>2</sub> three-phase composites.

There is an issue usually discussed in the study of ac-conductivity, which concerns the link between the values of the parameters  $n$  and  $A$  when the Jonscher's power law is applied [51], and the state of the material under study. Is there a direct relation between  $n$  and the state of the filler inside the sample (e.g., before and after percolation) or the sample morphology (e.g., two-phase, three-phase, filler aggregation or segregation process)? During this article, the authors aim to answer this question and link these parameters ( $n$  and  $A$ ) with the state of the material under investigation, in addition to studying some other properties. Also, an attempt to improve the distribution of carbon tubes with polymer by grinding and soaking it in the salt solution (to reduce the attractiveness of the MWCNTs between each other) before adding to the polymer as a kind of physical treatment. Also, adding salt to the host polymer will contribute significantly to improving the electrical properties of the nanocomposite. Therefore, the research will investigate the ac-conductivity for a group of two-phase (polymer electrolytic sample) and three-phase samples (polymer electrolyte loaded with MWCNTs) before and after percolation.

## 2 Experimental

### 2.1 Materials

Analytical-grade PVA (with average Mwt. of 130,000 and 99% degree of hydrolysis) as host polymer and Manganese(II) chloride hydrate (Mwt. of 125.84) were purchased from Aldrich. Functionalized MWCNTs were purchased from Chengdu Organic Chemicals Co. Ltd., China (diameter > 50 nm, 10–20 mm length, and purity > 95%).

### 2.2 Sample preparation

Three-phase polymer electrolyte nanocomposite samples (PVA + 5% MnCl<sub>2</sub> + x wt.% MWCNTs) were prepared using the cast techniques according to the following steps:

- 1 Specific weight of the polymer was dissolved in 15 ml of distilled water at 85 °C. The solution was continuously stirred using a magnetic stirrer for 3 h.
- 2 Manganese chloride salt was weighted to be about 5 wt.% of the total sample weight. The salt was dissolved in 10 ml of distilled water and then added to different weight ratios of MWCNTs (0.1, 0.4, 0.8, 1.0, 2.0 wt. %). The mixture was manually grinded in the MnCl<sub>2</sub> solution for 5 min (for MWCNTs untangling) and left for soaking (1 h) before adding the polymer solution. The three-phase solution was mixed using ultrasonicator for 2 h and transferred to a magnetic stirrer and stirred overnight (at ≈ 60 °C) to ensure the mixture homogeneity. The homogenous mixture was poured into flat glass plates and kept inside the thermal chamber (40–45 °C) and left to dry.

### 2.3 Dielectric measurements

The impedance (*Z*) and AC conductivity ( $\sigma_{ac}$ ) of the composites were measured using a Keithly 4200 SCS (Semiconductor Characterization System) at frequencies varying from 100 Hz to 10 MHz. Both *Z* and  $\delta$  (phase angle) were collected automatically after averaging then *Z'* (real part of impedance), *Z''* (imaginary part of impedance), and  $\sigma_{ac}$  (AC conductivity) were calculated. Copper conductive plates were used on both sides of the sample as conductive electrodes.

## 3 Discussion

Usually, pure polymers (other than conductive polymers) belong to the category of insulating materials due to the shortage of free-charge carriers. Therefore, their response to the applied AC field will be related to the dielectric relaxation effects which can be attributed to the transfer of space charges, the rotation of permanent dipoles in addition to the induced dipoles, segment mobility of polar groups, interfacial charge, as well as the relaxation due to transition of the materials from the glassy state to the rubber state. The addition of salts and/or nano-fillers may have an influence or impact on these relaxations process. Also, the interaction between the nano-fillers and polymer chains may cause a complex behavior for the relaxation process of the composite. The existence of induced polarization and interfacial polarization can also complicate the relaxation process.

The AC conductivity  $\sigma_{ac}$  can be calculated by the following relation:

$$\sigma_{ac} = 2\pi f \epsilon' \epsilon_0 \tan(\delta) \quad (1)$$

where  $\epsilon_0$  and  $\epsilon'$  are the dielectric constant of the free space and the material, respectively, and  $\tan(\delta)$  is the loss tangent or dissipation factor.

Figure 1 shows the frequency dependence of the AC conductivity ( $\sigma_{ac}$ ) at different temperatures (from 30 to 120 °C) for PVA, PVA/MnCl<sub>2</sub>, and PVA/MnCl<sub>2</sub>/MWCNTs samples. It is found that  $\sigma_{ac}$  increases with the increase in temperature (typical behavior for most insulating polymer) [52]. The increase in the temperature increases the mobility of charge carriers in the polymer matrix and polymer composite and also, increases the number of transit sites [51]. This will increase the ability of the charge carrier to transfer from one transit site to another and the charge carrier will be able to overcome the potential barrier to contribute in the conduction. It is noted that the frequency at which the dispersion occurs (hopping frequency  $\omega_H$ ) is shifted toward higher frequency as the temperature increases. In this case, it is possible to apply the Jonscher's power law (JPL) [51]:

$$\sigma_{ac}(\omega) = \sigma_{dc} + A\omega^n \quad (2)$$

where  $\omega$  is the angular frequency,  $\sigma_{dc}$  is the dc-conductivity (i.e., independent of frequency at  $\omega \cong 0$ ), **A** is a temperature-dependent constant, and **n** is an

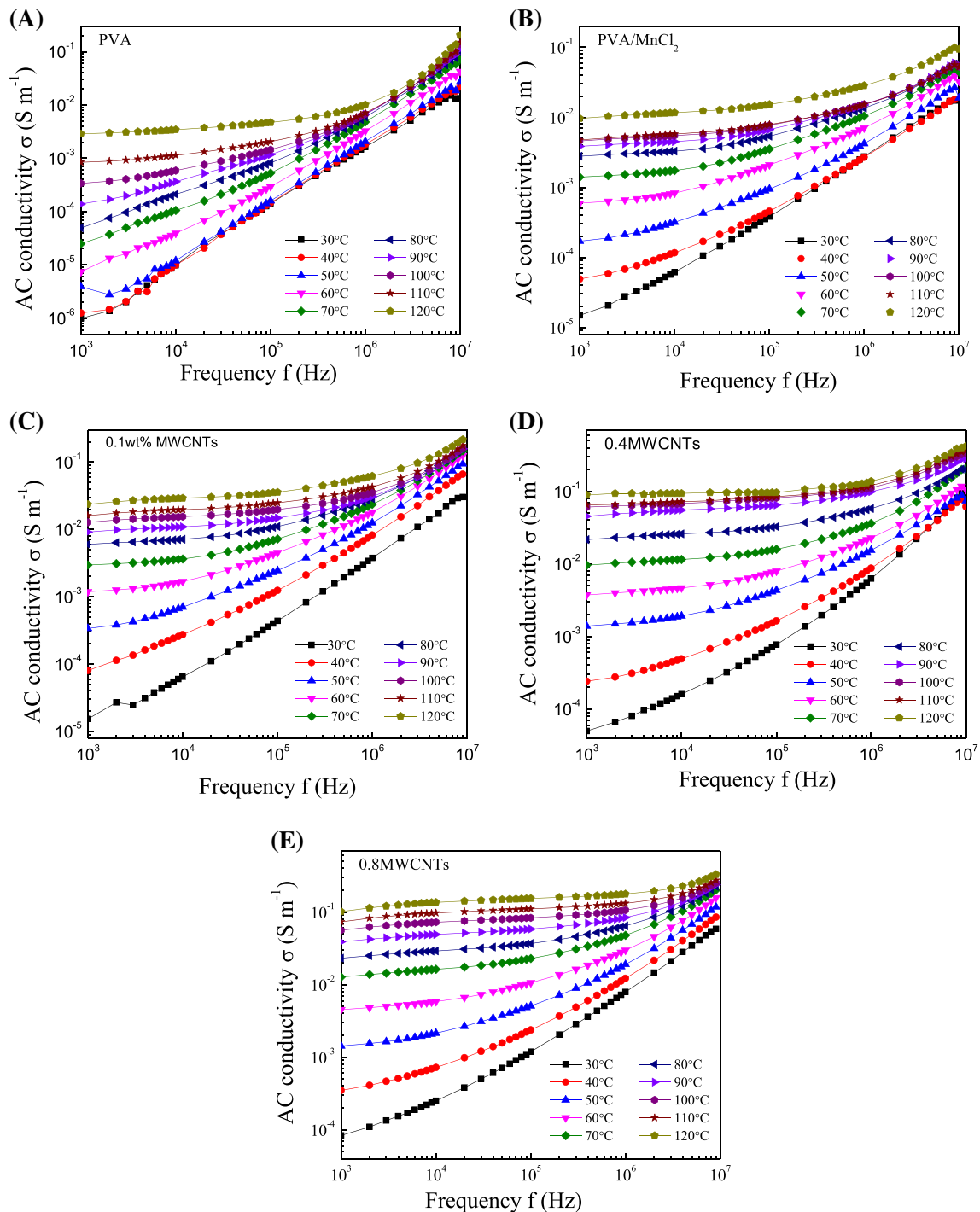


**Fig. 1** Variation of AC conductivity with frequency at different temperatures for PVA, PVA/MnCl<sub>2</sub>, and PVA/MnCl<sub>2</sub>/MWCNTs samples

exponent ( $0 \leq n \leq 1$ ). Both values ( $A$  and  $n$ ) depend on the temperature. The parameter  $A$  represents the strength of polarizability in the sample, whereas the parameter  $n$  represents the reactivity between the sample constituent (such as the interaction between the fillers with each other or the fillers with the

polymeric chains or the interaction of the polymeric chains with each other in the case of the polymer blend).

The variation of  $n$  with temperature depends on the type of conduction mechanism within the sample which depends on temperature, frequency, and

sample constituent. Quantum mechanical tunneling (QMT), correlated barrier hopping (CBH), non-overlapping small polaron tunneling (SPT), and overlapping large polaron tunneling (OLPT) are theoretical models that can be used to identify the conduction mechanism in the case of AC conductivity [53].

For pure PVA samples, the general Jonscher power law equation (Eq. 2) did not give a good fitting when applying the following initial conditions:  $\sigma_{ac} \geq 0$  and  $0 \leq n \leq 1$ , ; when using the modified Jonscher equation (Eq. 3) with the following initial conditions— $\sigma_{ac} \geq 0, 0 \leq n_1 \leq 1$ , and  $0 \leq n_2 \leq 2$ —a good fitting (Fig. 2) has been obtained.

$$\sigma_{ac} = \sigma_{ac} + A_1 \omega^{n_1} + A_2 \omega^{n_2} \tag{3}$$

For the two-phase sample (PVA/MnCl<sub>2</sub>), Jonscher power law (Eq. 2) was applied and it gives a good fitting (between 0.998 and 1).The temperature dependence of **n** and **A** is represented in Fig. 3a for the two-phase sample. The values of **n** decrease as temperature increases and it varied between 0.88 and 0.72 with average of 0.80. The constant **A** increases gradually with temperature and reach its maximum value at about 80 °C and then the values changed between  $4.35 \times 10^{-7}$  and  $3.12 \times 10^{-7}$ . The changes in the values of **n** and **A** (see Fig. 3a) indicate that, as the temperature increases (thermal activation), the polarizability increases (accumulation of the charge carriers and ions) in addition to the increase of the interfacial polarization. So, the ion–ion interaction and ion–polymer interaction decrease (i.e., **n** decreases). At near the glass transition temperature (T<sub>g</sub>), the chain mobility increases which in turn allows the

movement of ions and releases the accumulative charge carriers, which are reflected as reductions in the values of **A**.

The sample loaded with 0.1 wt.% MWCNTs (Fig. 3b) behaves similarly to the electrolytic sample (PVA/MnCl<sub>2</sub>). The general behavior of the constant **A** with temperature is a gradual increase, and near the glass transition the values of **n** oscillate around 0.93 and then continue to increase (reach to 1 at 120 °C). Moreover, the values of **n** behave almost opposite to the behavior of the parameter **A**. This behavior can be explained by following the same approach as the previous interpretation, as the sample is still before the percolation threshold.

Samples loaded with 0.4 wt.% and 0.8 wt.% MnCl<sub>2</sub> (Figs. 3c, d), which exceed the percolation threshold, have to some extent a different behavior where the value of **n** gradually decreased and then became almost constant over a wide range of temperatures (from 50 to 120 °C). For the sample loaded with 0.8wt%, **n** decreases gradually and increases dramatically above 100 °C. The constant **A** for both samples (0.4 wt.% and 0.8 wt.% MnCl<sub>2</sub>) shows a peak around 80 °C and is more symmetrical for the sample loaded with 0.8 wt.% MnCl<sub>2</sub>.

The behavior of samples after the percolation can be explained as follows:

1. Increasing the constant **A** with temperatures, below the glass transition temperature, may be due to the accumulation of ions and their lack of mobility. In addition, the presence of the

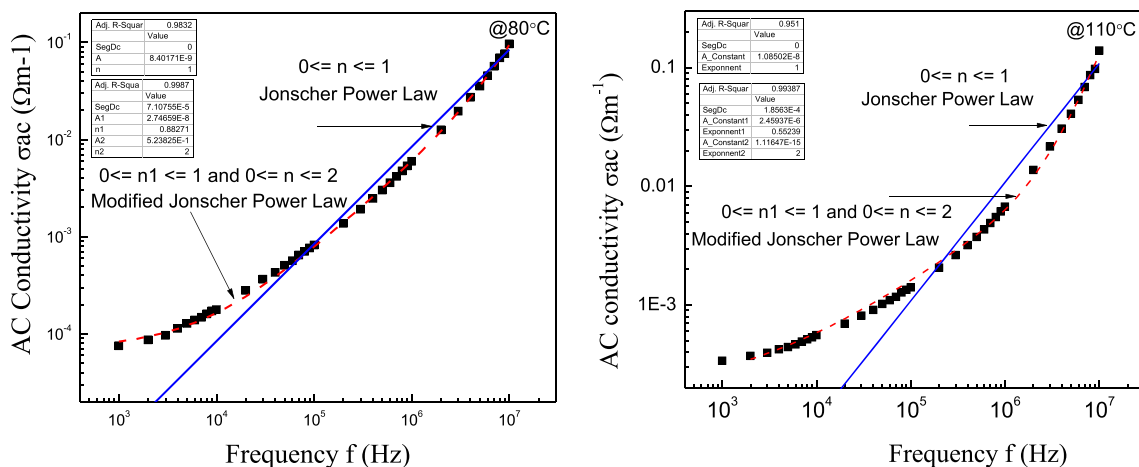


**Fig. 2** The frequency dependence of ac-conductivity for pure PVA at 80 and 110 °C. The full lines is given by JPL (Eq. 2) and broken lines are given by modified JPL (Eq. 3) with

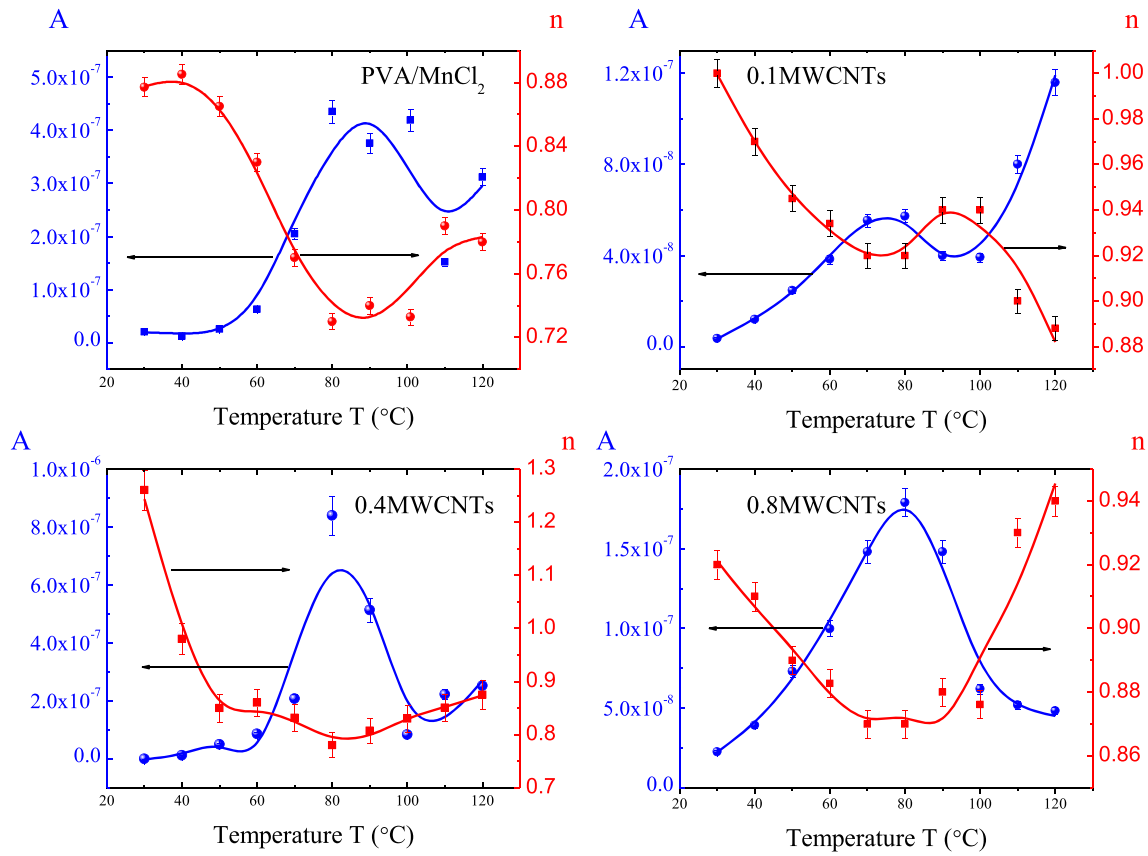


**Fig. 3** Variation of  $n$  exponent and  $A$  constant vs. temperature for PVA/MnCl<sub>2</sub> and PVA/MnCl<sub>2</sub>/MWCNTs samples

interfacial polarization around those ions will contribute to increasing the polarizability of the sample.

- At temperatures above the glass transition, the mobility of the polymeric chains will increase, allowing more mobility for the ions to contribute to the conduction process. As well as, the leakage of charges carriers, which contributes to the interfacial polarization, causes a decrease in the value of the constant  $A$  with temperature.
- Also, at high temperatures ( $T > T_g$ ) and as a result of the thermal expansion of the polymer in addition to the ease of movement of polymeric chains and charge carriers, the reactivity between the different elements will decrease, which is reflected as a decrease in the value of  $n$ . At temperatures greater than 100 °C, sample loaded with 0.8 wt.% can be excluded from this behavior, where  $n$  increases with increasing temperature. This can be attributed to the redistribution process of the filler and the formation of the filler aggregation.

By looking at the values of  $n$  and its temperature dependence, one can assume that the CBH model (which assume the charge carriers hop between two sites above the Coulomb barrier) to be the most predominant model for the samples under test, especially during temperatures below 100 °C, where the value of the parameter  $n$  decreases, and its values range between 0.8 and 1. However, for temperatures greater than 100 °C, the QMT model (which depends on phonon-assisted electron tunneling) is expected to be the most predominant conduction model.

Figure 4A–D represents the variation in AC conductivity versus frequency for pure, two-phase, and three-phase composite samples at 30, 60, 90, and 120 °C. It is seeming that the addition of MnCl<sub>2</sub> to PVA increases the AC conductivity. Also  $\sigma_{ac}$  increases with the increasing MWCNTs and there is an abrupt increase at 0.4 wt.% MWCNTs suggesting a percolation behavior. It is also noted that the addition of MWCNTs from 0.4 to 0.8 wt.% did not change the value of the AC conductivity particularly below 90 °C. This can be attributed to the uniform distribution of fillers within the electrolytic polymer and

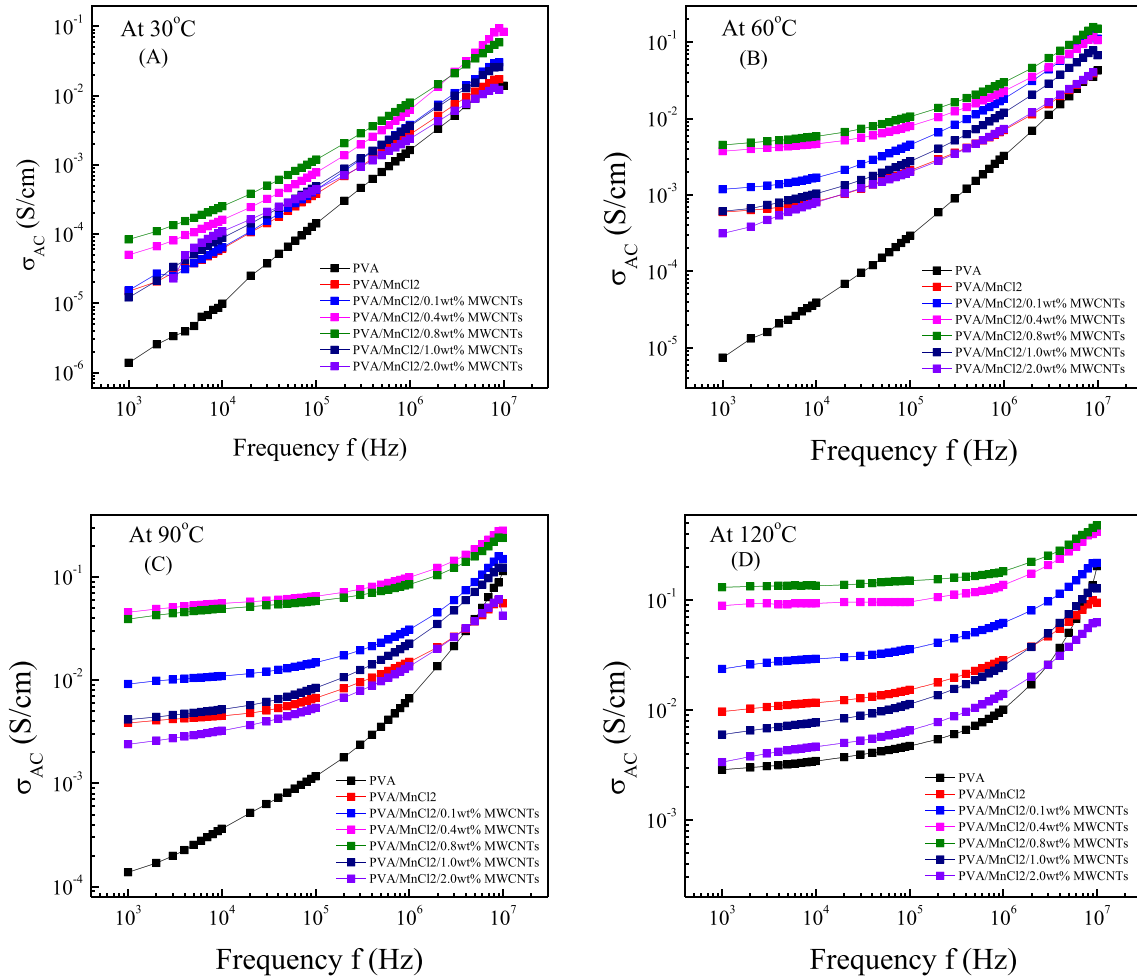


**Fig. 4** Variation of AC conductivity with frequency at different MWCNTs loading and fixed temperature for PVA/MnCl<sub>2</sub> and PVA/MnCl<sub>2</sub>/MWCNTs samples

that the presence of salt helped increase the degree of freedom of movement of the MWCNTs, which caused a uniform distribution of those fillers and reduce the percolation threshold.

When the concentrations of the MWCNTs exceed the 0.8 wt.%, it is noticed that the AC conductivity decreases, and this can be attributed to the formation of aggregates (due to the interaction of the fillers with each other) and the formation of conductive fillers islands separated by an insulating medium of the electrolytic polymer.

As the temperature increases a plateau region which is an indicator to the dc-conductivity contribution increases. This gradual change from dc plateau to (ac) dispersive region designates the distribution of relaxation times. The frequency dependence of electrical conductivity can be divided

into distinctive regions implying the existence of various dissipated effects [54].

Also, the increase of the AC conductivity at higher temperature (> 90 °C) can be attributed to the thermal expansion of the polymer matrix which leads to increase the chain mobility, encouraging the trapped ions to contribute in the conduction and hence increases the ionic conduction [52, 55]. The contribution of the segmental motion of the chains cannot neglect, since at temperatures above the glass transition the mobility of the chain increases and the chain segment contributes directly in the conduction mechanism.

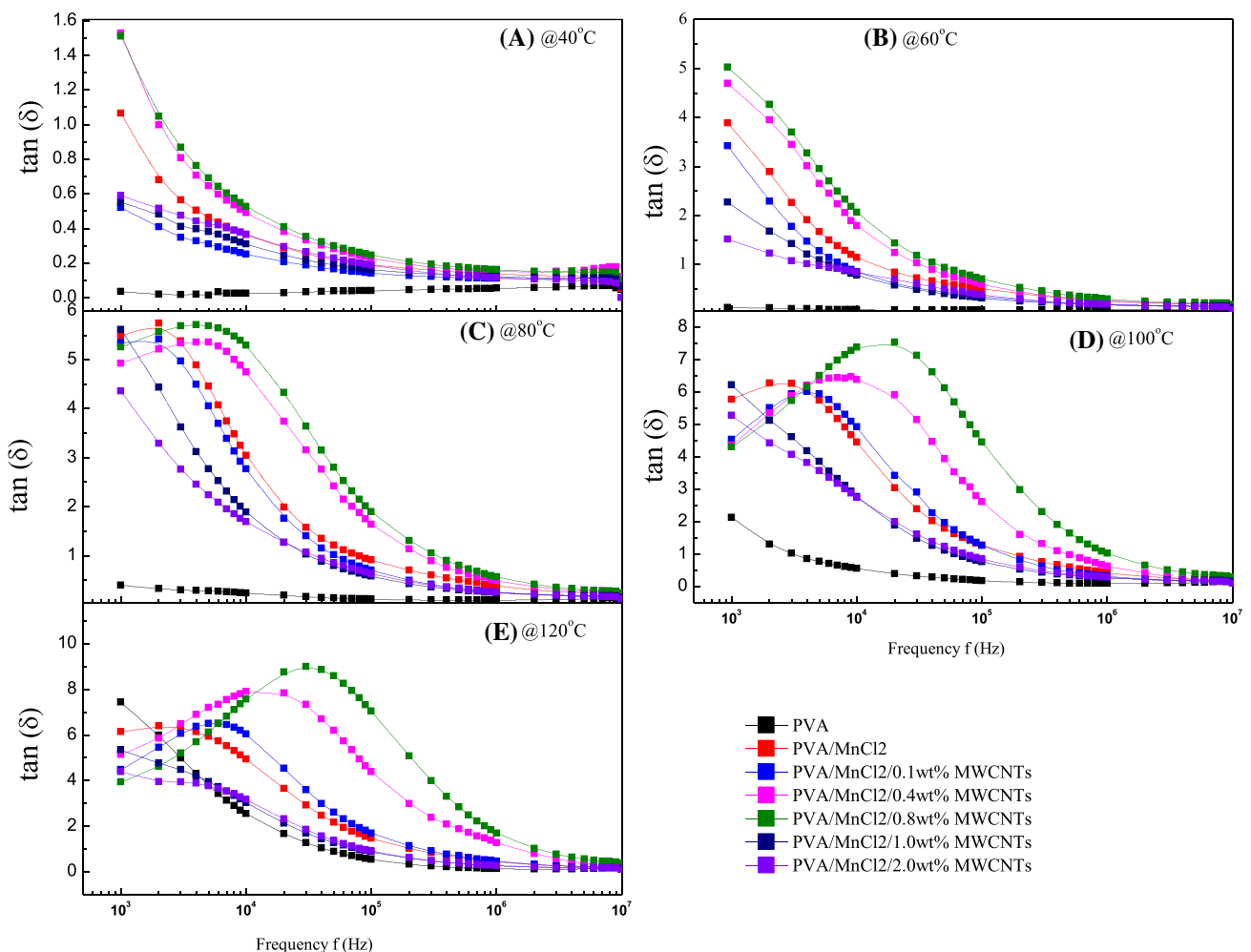
It is known that the dielectric loss arises from the dissipation of the acquired energy during the charge or electric dipole movement in an alternating electric field. This energy loss is due to the phase lag between the charge or dipole response and the applied field.

Figure 5 shows the loss factor ( $\tan \delta$ ) for the two-phase and three-phase samples at different temperatures. The dielectric loss curves for the samples follow the typical behavior, where the loss decreases gradually as the frequency increases. This behavior can be explained by considering the response of the charges and dipoles to the applied electric field at low and high frequencies. When the field frequency is low, the response of the charges (or dipoles) to the electric field will be high, so the loss factor is also high. The loss gradually decreases with increasing frequency, due to the weak response of field dipoles. This behavior depends on the nature of the sample, frequency range, and temperature. In the present case, Maxwell–Wagner–Sillars (MWS) interfacial polarization represents the main source of dielectric loss at low frequency [56].

The dielectric loss increases with increasing loading of MWCNTs up to 0.8 wt.% and then decreases sharply for 1 wt.% and 2 wt.% loaded samples. This change can be interpreted as follows:

1. Above the percolation threshold, the dielectric loss increases due to the formation of a network of capacitors and resistors through the sample, and these components are randomly connected in series and parallel [57].
2. When the loading of MWCNTs exceeds a certain level, the formation of MWCNTs aggregation (isolated islands) will occur and the number of micro-capacitors and resistors will decrease. Therefore, the dielectric loss will also decrease.

It is also noted that, for temperatures above  $T_g$ , the loss spectra were characterized by a definite peak for samples loaded with MWCNTs up to 0.8 wt.%. These



**Fig. 5** Variation of  $\tan(\delta)$  with frequency at different MWCNTs loading and fixed temperature for PVA/MnCl<sub>2</sub> and PVA/MnCl<sub>2</sub>/MWCNTs samples



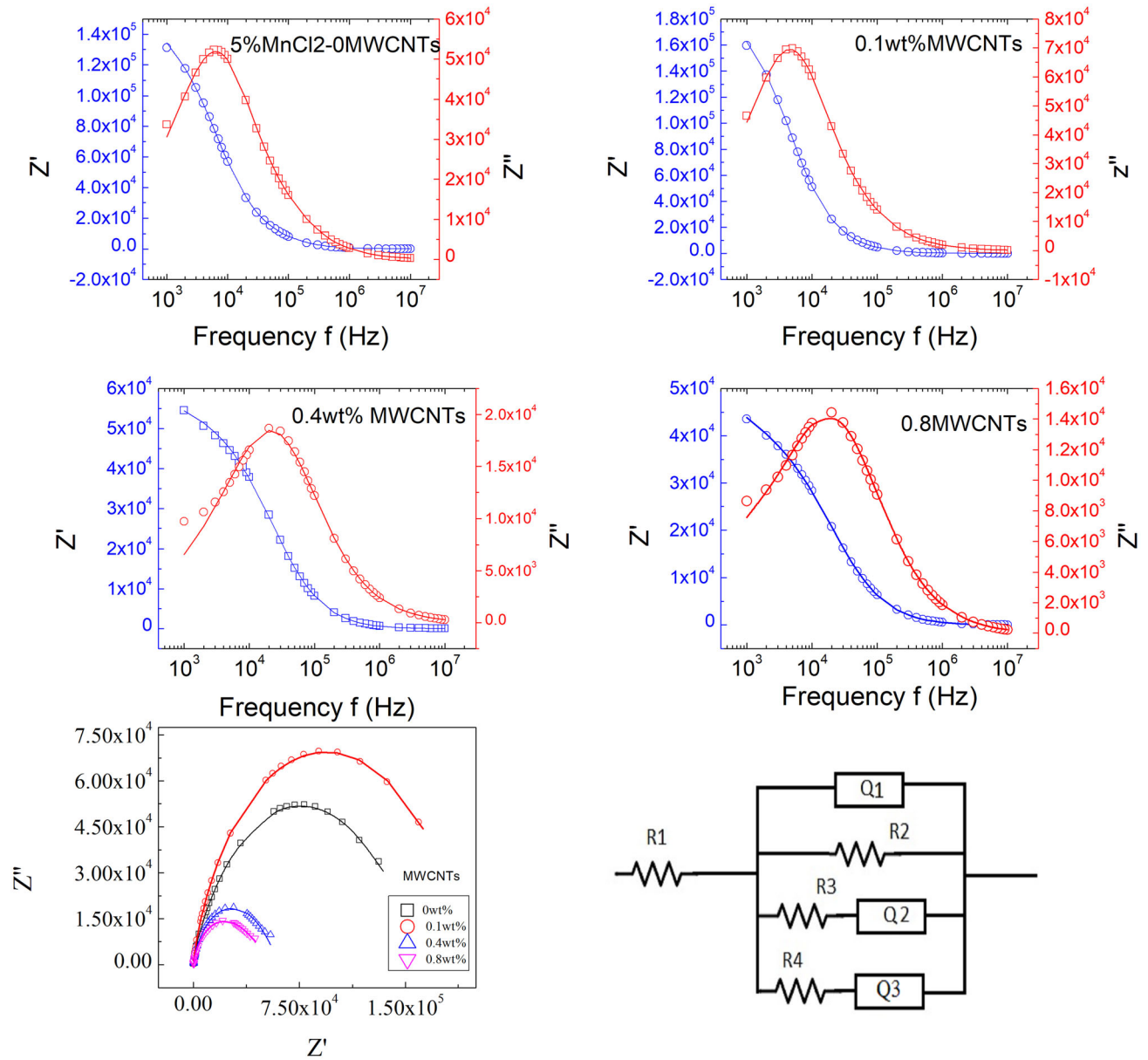


**Fig. 6** Cole–Cole fit of two- and three-phase samples at 60 °C; the open symbols are the experimental data and the solid lines are the fitted curves

peaks shifted toward higher frequency with MWCNTs loading, indicating that the relaxation time decreases on increasing MWCNTs loading. This can be attributed to the fact that within the percolation region, the resistive and capacitive components of the networks decrease as the filler loading increases (before aggregation formation) reducing the relaxation time. A noticeable shift for the loss tangent peak toward the higher frequency side with temperature increase is attributed to the thermal activation of the charge and electric dipoles [58, 59].

Zsimwin program was used to find the equivalent circuit of the samples. Figures 6 and 7 show the fitting between the theoretical and experimental values of the two-phase (PVA/MnCl<sub>2</sub>) and three-phase (PVA/MnCl<sub>2</sub>/MWCNTs) samples at temperatures 60 and 100 °C as representative results.

The equivalent circuit depicted in Fig. 3 is employed to analyze the impedance.

The equivalent circuits depicted in Fig. 8A, B are employed to analyze the impedance spectra for the two- and three-phase samples. In both circuits, R<sub>1</sub>

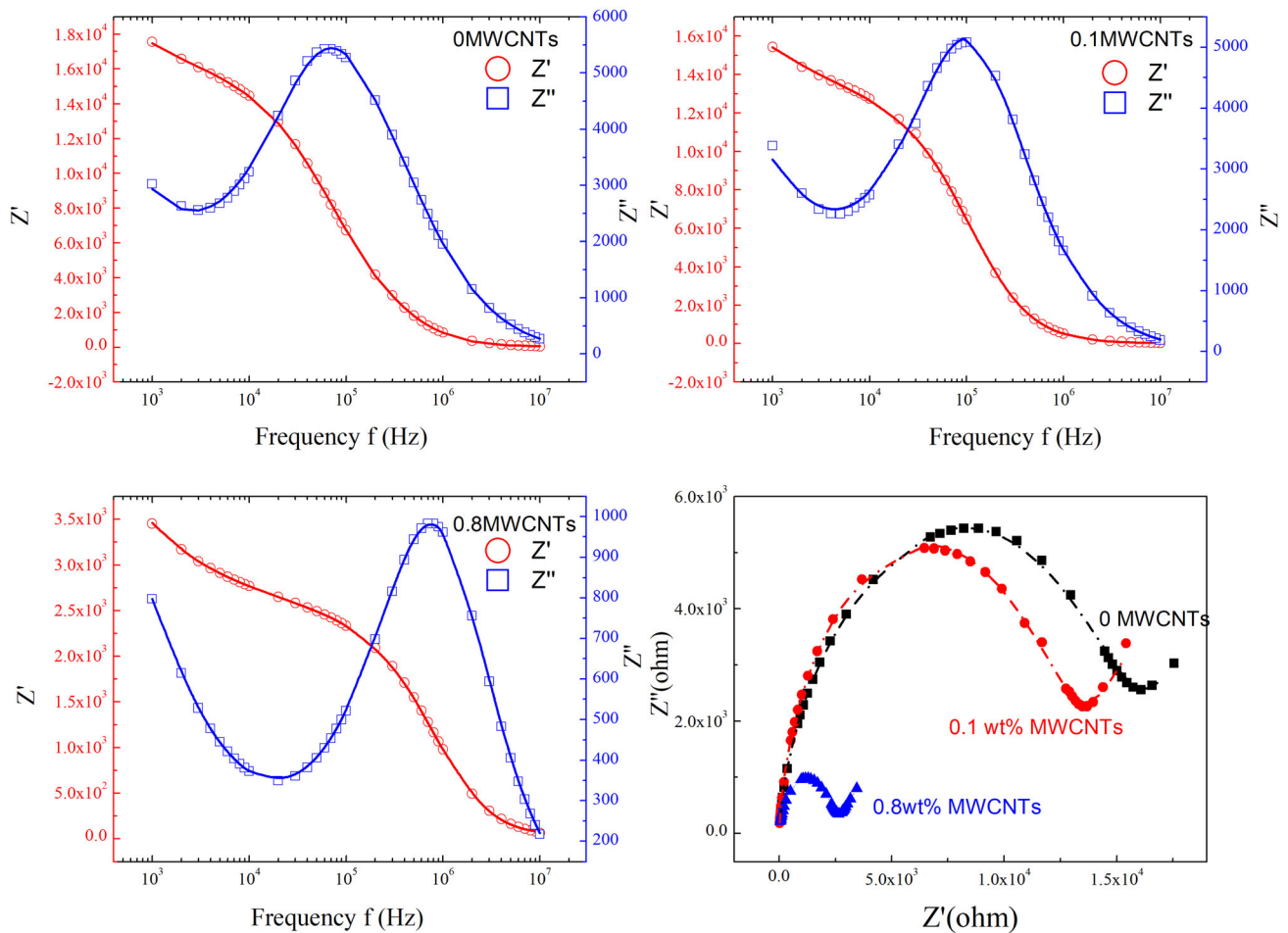
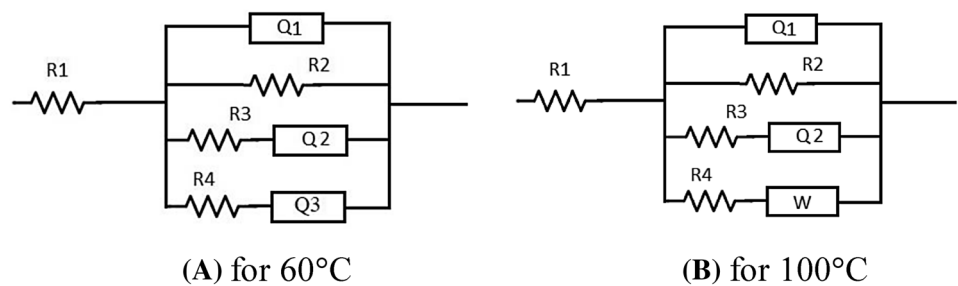


**Fig. 7** Cole–Cole fit of two- and three-phase samples at 100 °C; the open symbols are the experimental data and the solid lines are the fitted curves

**Fig. 8** Electrical equivalent circuit model representing impedance spectra to fit the experimental complex impedance, for two- and three-phase samples



represents the electrode resistance, placed in series with the resistance of the polymer media ( $R_2$ ).  $Q_1$  is the imperfect capacitance due to the dielectric nature of the polymer media,  $R_3$  is the resistance to the transfer of charge through the electrolytic media and  $Q_2$  is a constant phase element representing the capacity of the interfacial polarization at the interface between the MWCNTs and the electrolyte, while  $R_4$

and  $Q_3$  represent the resistance to the transfer of charge between MWCNTs and the constant phase element (capacitance) between the MWCNTs aggregates at temperature 60 °C. At 100 °C and due to thermal expansion the CPE connected with  $R_4$  will change to  $W$  which represents the diffusion of charge between the MWCNTs aggregates.

## 4 Conclusion

Casting techniques has been utilized for the preparation of two-phase and three-phase electrolyte nanocomposite samples (PVA/MnCl<sub>2</sub> and PVA/MnCl<sub>2</sub>/MWCNTs). The samples were loaded with different weight ratios of MWCNTs (0.1, 0.4, 0.8, 1.0, 2.0 wt. %). The results investigate the dielectric properties for the two- and three-phase samples within the frequency range of 100–1\*10<sup>6</sup> Hz and at various temperatures (30 to 120 °C). The addition of MWCNTs to the electrolyte sample significantly improved the electrical conductivity of the composite (e.g., about three orders of magnitude at 500 Hz at 60°). A sudden increase was observed at 0.4 wt.% MWCNTs indicating leaching behavior. The ac-conductivity spectra were following Jonscher's power law. For PVA/MnCl<sub>2</sub> sample, the values of n (exponent) decreased as temperature increased and varied between 0.88 and 0.72 with an average of 0.80. Above the percolation threshold, the variation of n and A was interpreted by considering the redistribution of the accumulated charges (close to T<sub>g</sub>) beside the change in the ions mobility and polymeric chains. The CBH model is the most predicted model for the samples under test, especially at temperatures below 100 °C, where the parameter n values decrease and range from 0.8 to 1. However, the QMT model is predicted to be the most prevalent conduction model for temperatures greater than 100 °C.

## Acknowledgements

This work was supported by the Deanship of Scientific Research, Vice Presidency for Graduate Studies and Scientific Research, King Faisal University, Saudi Arabia [Grant No. 973].

## Author contributions

All authors contributed to the study conception and design. Material preparation, data collection, and analysis were performed by SSI. The first draft of the manuscript was written by HA and the two authors commented on previous versions of the manuscript. All authors read and approved the final manuscript.

## Data availability

The data that support the findings of this study are available from the corresponding author on reasonable request.

## Declarations

**Competing interest** The authors have no relevant financial or non-financial interest to disclose.

**Open Access** This article is licensed under a Creative Commons Attribution 4.0 International License, which permits use, sharing, adaptation, distribution and reproduction in any medium or format, as long as you give appropriate credit to the original author(s) and the source, provide a link to the Creative Commons licence, and indicate if changes were made. The images or other third party material in this article are included in the article's Creative Commons licence, unless indicated otherwise in a credit line to the material. If material is not included in the article's Creative Commons licence and your intended use is not permitted by statutory regulation or exceeds the permitted use, you will need to obtain permission directly from the copyright holder. To view a copy of this licence, visit <http://creativecommons.org/licenses/by/4.0/>.

## References

1. H. Wu et al., Stable cycling of double-walled silicon nanotube battery anodes through solid-electrolyte interphase control. *Nat. Nanotechnol.* **7**(5), 310–315 (2012)
2. Q. Lu, J. Fang, J. Yang, G. Yan, S. Liu, J. Wang, A novel solid composite polymer electrolyte based on poly (ethylene oxide) segmented polysulfone copolymers for rechargeable lithium batteries. *J. Membr. Sci.* **425**, 105–112 (2013)
3. N. Cioffi et al., Copper nanoparticle/polymer composites with antifungal and bacteriostatic properties. *Chem. Mater.* **17**(21), 5255–5262 (2005)
4. P. Hine, V. Broome, I. Ward, The incorporation of carbon nanofibres to enhance the properties of self reinforced, single polymer composites. *Polymer* **46**(24), 10936–10944 (2005)
5. A. Peláiz-Barranco, P. Marin-Franch, Piezo-, pyro-, ferro-, and dielectric properties of ceramic/polymer composites obtained from two modifications of lead titanate. *J. Appl. Phys.* **97**(3), 034104 (2005)

6. A. Ostendorf, M.B. Chakif, Q. Guo, Laser direct writing of nanocompounds, in *MRS proceedings*. (Cambridge Univ Press, Cambridge, 2011)
7. G. Hernandez-Sosa et al., The role of the polymer solid electrolyte molecular weight in light-emitting electrochemical cells. *Org. Electron.* **14**(9), 2223–2227 (2013)
8. S. Zekoll et al., Hybrid electrolytes with 3D bicontinuous ordered ceramic and polymer microchannels for all-solid-state batteries. *Energy Environ. Sci.* **11**, 185–201 (2018)
9. F. Chen, W. An, Y. Li, Y. Liang, W. Cui, Fabricating 3D porous PANI/TiO<sub>2</sub>–graphene hydrogel for the enhanced UV-light photocatalytic degradation of BPA. *Appl. Surf. Sci.* **427**, 123–132 (2018)
10. C. Ren, M. Liu, J. Zhang, Q. Zhang, X. Zhan, F. Chen, Solid-state single-ion conducting comb-like siloxane copolymer electrolyte with improved conductivity and electrochemical window for lithium batteries. *J. Appl. Polym. Sci.* **135**(9), 45848 (2018)
11. M.S. Thomas, S.P. White, K.D. Dorfman, C.D. Frisbie, Interfacial charge contributions to chemical sensing by electrolyte-gated transistors with floating gates. *J. Phys. Chem. Lett.* **9**(6), 1335–1339 (2018)
12. T.-Y. Kim et al., Poly (3,4-ethylenedioxythiophene) quantum dot-sensitized solar cells in the solid-state utilizing polymer electrolyte. *ACS Appl. Energy Mater.* **1**(2), 290–295 (2018)
13. T. Nguyen, J.J. Magda, P. Tathireddy, Manipulation of the isoelectric point of polyampholytic smart hydrogels in order to increase the range and selectivity of continuous glucose sensors. *Sens. Actuators B Chem.* **255**, 1057–1063 (2018)
14. A. Giovannitti et al., The role of the side chain on the performance of N-type conjugated polymers in aqueous electrolytes. *Chem. Mater.* **30**(9), 2945–2953 (2018)
15. C.S. Abreu, D.S.C. Neves, V.A. Gomes, A.B. Mageste, G.D. Rodrigues, L.R. de Lemos, Aqueous three-phase systems formed by poly (vinylpyrrolidone)+ poly (ethyleneglycol)+ lithium sulfate+ water: phase behavior and partition data. *J. Mol. Liq.* **355**, 118959 (2022)
16. M.O.H. Schutzeichel, T. Kletschkowski, H.P.J.F.C. Monner, Effective stiffness and thermal expansion of three-phase multifunctional polymer electrolyte coated carbon fibre composite materials. *Funct. Compos. Struct.* **3**(1), 015009 (2021)
17. T. Somesh, T.J.J.O.S.S.C. Demappa, Tailoring of ternary nanocomposite films of poly (vinyl alcohol)/AgAlO<sub>2</sub>@ reduced graphene oxide: an active material for flexible supercapacitors. *J. Solid State Chem.* **309**, 122824 (2022)
18. B.X. Rutherford et al., Tunable three-phase Co–CeO<sub>2</sub>–BaTiO<sub>3</sub> hybrid metamaterials with nano-mushroom-like structure for tailorable multifunctionalities. *ACS Appl. Nano Mater.* **5**(5), 6297–6304 (2022)
19. M. Pandey, K. J. G. N. Deshmukh (2022) Novel three phase dielectric composites comprising cerium oxide nanoparticles, graphene nanoplatelets and poly (vinylidene fluoride)
20. L. Liu, D. Wang, J. Huang, Z. Huang, Y. Zhang, L.J.A.O. Li, Multicomponent composite membrane with three-phase interface heterostructure as photocatalyst for organic dye removal. *ACS Omega* **7**(20), 17128–17143 (2022)
21. M. Shoorangiz, Z. Sherafat, E.J.C.I. Bagherzadeh, CNT loaded PVDF-KNN nanocomposite films with enhanced piezoelectric properties. *Ceram. Int.* **48**(11), 15180–15188 (2022)
22. L. Yuan et al., Flexible solid-state supercapacitors based on carbon nanoparticles/MnO<sub>2</sub> nanorods hybrid structure. *ACS Nano* **6**(1), 656–661 (2011)
23. S. Venkatesan et al., Nanomaterials and films for polymer electrolyte membrane fuel cells and solid oxide cells by flame spray pyrolysis. *Renew. Sustain. Energy Rev.* **158**, 112080 (2022)
24. Y. Iwahori, S. Ishiwata, T. Sumizawa, T. Ishikawa, Mechanical properties improvements in two-phase and three-phase composites using carbon nano-fiber dispersed resin. *Compos. A Appl. Sci. Manuf.* **36**(10), 1430–1439 (2005)
25. S. Rana, R. Alagirusamy, M. Joshi, Development of carbon nanofibre incorporated three phase carbon/epoxy composites with enhanced mechanical, electrical and thermal properties. *Compos. A Appl. Sci. Manuf.* **42**(5), 439–445 (2011)
26. X. Song et al., Cu nanoparticles improved thermal property of form-stable phase change materials made with carbon nanofibers and LA-MA-SA eutectic mixture. *J. Nanosci. Nanotechnol.* **18**(4), 2723–2731 (2018)
27. N.R. Chodankar, S.-H. Ji, D.-H. Kim, Low-cost superior symmetric solid-state supercapacitors based on MWCNTs/MnO<sub>2</sub> nanocomposite thin film. *J. Taiwan Inst. Chem. Eng.* **80**, 503–510 (2017)
28. H. Kim, J. Johnson, L.A. Chavez, C.A.G. Rosales, T.-L.B. Tseng, Y. Lin, Enhanced dielectric properties of three phase dielectric MWCNTs/BaTiO<sub>3</sub>/PVDF nanocomposites for energy storage using fused deposition modeling 3D printing. *Ceram. Int.* **44**(8), 9037–9044 (2018)
29. F. Zhong et al., Modification of sulfonated poly (etherether ketone) composite polymer electrolyte membranes with 2D molybdenum disulfide nanosheet-coated carbon nanotubes for direct methanol fuel cell application. *Polymer* **249**, 124839 (2022)
30. J. Kim et al., High-performance polymer electrolyte membrane fuel cells with nanoporous carbon nanotube layer in low humidity condition. *J. Power Sources* **537**, 231416 (2022)
31. M.Q. Al-Gunaid, A. Saeed, Effects of the electrolyte content on the electrical permittivity, thermal stability, and optical dispersion of poly (vinyl alcohol)–cesium copper oxide–

- lithium perchlorate nanocomposite solid-polymer electrolytes. *J. Appl. Polym. Sci.* **135**(8), 45852–45852 (2018)
32. K. Jagatheesan, A. Ramasamy, A. Das, A. Basu, Electromagnetic absorption behaviour of ferrite loaded three phase carbon fabric composites. *Smart Mater. Struct.* **27**(2), 025004 (2018)
  33. A.D. Sekar, H. Muthukumar, N.I. Chandrasekaran, M. Matheswaran, Photocatalytic degradation of naphthalene using calcined Fe-ZnO/PVA nanofibers. *Chemosphere* **205**, 610–617 (2018)
  34. P. Upasani, T. Sreekumar, V. Gaikar, N. Jha, Preparation of ZnO/MWCNT/PP composite film and its application as multifunctional protective film. *Polym. Compos.* **39**(1), 157–170 (2018)
  35. S. Sadeghi, A. Mollahosseini, Electrospun polydimethylsiloxane/polyacrylonitrile/titanium dioxide nanofibers as a new coating for determination of alpha-linolenic acid in milk by direct immersion-solid phase nanoextraction. *J. Chromatogr. B* **1073**, 43–50 (2018)
  36. M. Yang et al., Thermal and electrical properties of BNNPs/TiO<sub>2</sub>-epoxy three-phase nanocomposites, in *1st international conference on electrical materials and power equipment (ICEMPE)*. (Piscataway, IEEE, 2017), pp.540–543
  37. S. Guana, H. Li, S. Zhao, L. Guo, Novel three-component nanocomposites with high dielectric permittivity and low dielectric loss co-filled by carboxyl-functionalized multi-walled nanotube and BaTiO<sub>3</sub>. *Compos. Sci. Technol.* **158**, 79–85 (2018)
  38. N. Lakshmi, P. Tambe, N.K. Sahu, Giant permittivity of three phase polymer nanocomposites obtained by modifying hybrid nanofillers with polyvinylpyrrolidone. *Compos. Interfaces* **25**(1), 47–67 (2018)
  39. M. Moussa et al., Development of flexible supercapacitors using an inexpensive graphene/PEDOT/MnO<sub>2</sub> sponge composite. *Mater. Des.* **125**, 1–10 (2017)
  40. A.S. Zeraati, M. Arjmand, U. Sundararaj, Silver nanowire/MnO<sub>2</sub> nanowire hybrid polymer nanocomposites: materials with high dielectric permittivity and low dielectric loss. *ACS Appl. Mater. Interfaces* **9**(16), 14328–14336 (2017)
  41. B.C. Nath et al., High performance polyvinyl alcohol/multi walled carbon nanotube/polyaniline hydrogel (PVA/MWCNT/PAni) based dye sensitized solar cells. *Electrochim. Acta* **146**, 106–111 (2014)
  42. S. Ibrahim, A.S. Ayesh, Electrical and optical properties of functionalized multiwalled carbon nanotubes/poly (3-octylthiophene)/polystyrene composites. *J. Thermoplast. Compos. Mater.* **28**(2), 225–240 (2015)
  43. C. Meng, C. Liu, L. Chen, C. Hu, S. Fan, Highly flexible and all-solid-state paperlike polymer supercapacitors. *Nano Lett.* **10**(10), 4025–4031 (2010)
  44. W.-H. Pan, S.J. Lue, C.-M. Chang, Y.-L. Liu, Alkali doped polyvinyl alcohol/multi-walled carbon nano-tube electrolyte for direct methanol alkaline fuel cell. *J. Membr. Sci.* **376**(1), 225–232 (2011)
  45. Q.-M. Tu et al., Design of a novel redox-active gel polymer electrolyte with a dual-role ionic liquid for flexible supercapacitors. *Electrochim. Acta* **268**, 562–568 (2018)
  46. G. Zhou et al., Highly sensitive wearable textile-based humidity sensor made of high-strength, single-walled carbon nanotube/poly(vinyl alcohol) filaments. *ACS Appl. Mater. Interfaces* **9**(5), 4788–4797 (2017)
  47. S. Yu et al., Excellent thermostable and mechanically reinforced lithium-ion capacitor based on inverse opal structural PVDF-HFP/MWCNT electrolyte. *ACS Appl. Energy Mater.* **5**(3), 3876–3885 (2022)
  48. M. Sultana, U. Mehmood, R. Nazar, Y.Q. Gill, Development of multiwalled carbon nanotubes/polyaniline nanocomposites based electrolyte for quasi-solid-state dye-sensitized solar cells. *Int. J. Energy Res.* **46**(7), 9911–9918 (2022)
  49. M. Frank, J. Pflaum, Tuning electronic and ionic transport by carbon-based additives in polymer electrolytes for thermoelectric applications. *Adv. Funct. Mater.* **32**, 2203277 (2022)
  50. A. Mohammed, M. Hammed, M. Hasan Suhail, Electrical properties of PVA:PEG/MnCl<sub>2</sub> thin film composites. *Iraqi J. Phys.* **15**(33), 122–130 (2019)
  51. A.K.J.J.O.P.D.A.P. Jonscher, Dielectric relaxation in solids. *J. Phys. D Appl. Phys.* **32**(14), R57 (1999)
  52. R. Baskaran, S. Selvasekarapandian, N. Kuwata, J. Kawamura, T.J.M.C. Hattori, Ac impedance, DSC and FT-IR investigations on (x) PVAc–(1–x) PVdF blends with LiClO<sub>4</sub>. *Mater. Chem. Phys.* **98**(1), 55–61 (2006)
  53. M. Sassi, A. Bettaïbi, A. Oueslati, K. Khirouni, M.J.J.O.A. Gargouri, Compounds, electrical conduction mechanism and transport properties of LiCrP<sub>2</sub>O<sub>7</sub> compound. *J. Alloys Compd.* **649**, 642–648 (2015)
  54. A.J.I. Von Hippel, *Dielectrics and waves* (Artech House, Norwood, 1995)
  55. J.S. Wilkes, J.A. Levisky, R.A. Wilson, C.L.J.I.C. Hussey, Dialkylimidazolium chloroaluminate melts: a new class of room-temperature ionic liquids for electrochemistry, spectroscopy and synthesis. *Inorg. Chem.* **21**(3), 1263–1264 (1982)
  56. P. J. H. Hedvig, *Dielectric Spectroscopy in Polymers*, edited by A, vol. 283
  57. B. Chaudhuri, S. Ghosh, B. Mondal, D. Bhadra, Preparation and characterization of carbon fibre powder (CFP)-polyvinyl alcohol (PVA) composite films showing percolation threshold behaviour. *Mater. Sci. Eng. B* **275**, 115500 (2022)
  58. L. Fan, Z. Dang, G. Wei, C.-W. Nan, M.J.M.S. Li, Effect of nanosized ZnO on the electrical properties of (PEO)

- 16LiClO<sub>4</sub> electrolytes. *Mater. Sci. Eng. B* **99**(1–3), 340–343 (2003)
59. V. Mohan, W. Qiu, J. Shen, W.J.J.O.P.R. Chen, Electrical properties of poly (vinyl alcohol)(PVA) based on LiFePO<sub>4</sub> complex polymer electrolyte films. *J. Polym. Res.* **17**(1), 143–150 (2010)

**Publisher's Note** Springer Nature remains neutral with regard to jurisdictional claims in published maps and institutional affiliations.